



A facile process to prepare fouling-resistant ultrafiltration membranes: Spray coating of water-containing block copolymer solutions on macroporous substrates

Dongwei Ma^a, Xiangyue Ye^a, Zhuo Li^a, Jiemei Zhou^{a,*}, Dinglei Zhong^a, Chenxu Zhang^a, Sen Xiong^a, Jianzhong Xia^{b,c,*}, Yong Wang^{a,*}

^a State Key Laboratory of Materials-Oriented Chemical Engineering, College of Chemical Engineering, Nanjing Tech University, Nanjing 211816, Jiangsu, China

^b Institute for Advanced Study, Shenzhen University, Shenzhen 518060, Guangdong, China

^c Beijing OriginWater Membrane Technology Co., Ltd., Beijing 101407, China

ARTICLE INFO

Keywords:

Spray coating
Block copolymer
Nonsolvent induced phase separation
Ultrafiltration membrane

ABSTRACT

Ultrafiltration membranes derived from block copolymers (BCPs) are gaining much attention for their superiority in tunable pore structures and intrinsic surface functions. In terms of the practical applications of BCP membranes, simple and efficient manufacturing processes are essential and remain highly demanded. Herein, we propose a facile process to prepare BCP composite membranes by spray-coating polysulfone/poly(ethylene glycol) (PSF-*b*-PEG) solutions onto macroporous substrates. A small amount of nonsolvent (water) is added into the BCP solutions to act as the pore-forming agent. During spray coating, the evaporation of solvent and the rising water content lead to phase separation of BCP solutions in the atomized droplets. Subsequent drying removes water, and the volumes occupied by water are transformed into nanoscale pores, thus producing bilayered composite membranes with the nanoporous BCP coatings as the selective layers atop the macroporous substrates. Water-affinitive PEG chains in PSF-*b*-PEG are crucial to adsorb and stabilize water droplets during pore formation. The thickness of the BCP selective layers is predominantly determined by the dosage of the sprayed BCP solutions, enabling tunable separation properties of the BCP membranes. In spite of the extremely simple preparation process, thus produced membranes exhibit good ultrafiltration performances, comparable or better than that of membranes prepared by much more complicated processes. Furthermore, PEG chains are enriched on pore walls, endowing the membranes an intrinsic fouling resistance.

1. Introduction

Polymeric membranes have emerged as the core part in the fields of water treatments, pharmaceutical and food industries, desalination and energy storage [1–3], primarily owing to their advantages of low energy consumption, environmental friendliness, easy processing and high flexibility. The materials and methods for polymeric membrane manufacturing, which determine the performances of membranes, have become the primary focus of researches in recent years. Block copolymers (BCPs) are a class of peculiar polymeric materials that are composed of two or more covalently connected chains with distinct repeating units [4]. The thermodynamic incompatibility of different chains leads to the phase separation of BCPs on the nano scale (~10–50 nm) [5]. Abetz and Peinemann et al. [6,7] combined the self-assembly of

BCPs with the non-solvent induced phase separation (SNIPS) to produce asymmetric membranes with regular surface pores and narrow pore size distribution, which is a promising method for practical applications. Besides, by transforming the dispersed phases into pores, BCPs show great advantages on producing ultrafiltration (UF) membranes with highly ordered nanoporosities. A number of strategies have been reported to produce porous membranes from BCPs precursors [8–11]. The direct way is chemically degrading the microdomains of minority blocks in the phase-separated BCPs to produce highly uniform pores, namely selective etching [12,13]. This method is specifically limited to the BCPs with chemically labile minority blocks like poly(methyl methacrylate) (PMMA) [14], polylactide (PLA) [15], poly(dimethylsilane) (PDMS) [16], etc. Alternatively, our group has demonstrated a nondestructive physical method to create pores by immersing BCP films into selective

* Corresponding authors.

E-mail addresses: zhoujm@njtech.edu.cn (J. Zhou), xiajianzhong@outlook.com (J. Xia), yongwang@njtech.edu.cn (Y. Wang).

<https://doi.org/10.1016/j.seppur.2020.118100>

Received 22 September 2020; Received in revised form 5 November 2020; Accepted 12 November 2020

Available online 26 November 2020

1383-5866/© 2020 Elsevier B.V. All rights reserved.

solvents, which is termed as selective swelling induced pore generation [17]. It comes to be a more convenient way to produce porous BCP membranes. Despite these existing strategies, unceasing pursuit of innovative and efficient fabrication strategies for the production of porous membranes from BCPs precursors still remains high demanded.

From the aspect of practical applications, composite membranes with the nanoporous BCP separation layers atop the macroporous supporting layers are more attractive compared to the self-standing BCP membranes. They can not only substantially reduce the usage of costly BCPs, but also promote the permeance and maintain the mechanical robustness. There are some approaches to coat thin BCP layers on the porous supports to construct composite membranes, for instance, transferring and direct coating [18]. The former is producing thin BCP layers on solid substrates [19] or liquid surface [20] firstly, and then transfers the BCP layers onto microfiltration (MF) membranes, thus forming composite membranes. However, the manual transferring process is uncontrollable and susceptible to cause cracks due to the fragility of such thin films. This transferring process is much productive and reproducible under the assistant of transfer tool and drain chamber [21]. The latter approach constructs thin BCP layers by casting [22], drop coating [23] or vacuum filtration [24] of BCP solutions on porous substrates directly. To prevent the leakage of BCP solutions, this approach always involves pretreatment of substrates or needs the assistant of transitional layers, which is also tedious and hard to control. Therefore, there is an urgent demand to develop alternative methods that can radically simplify the manufacturing process and be applicable to the upscalable preparation of BCP composite membranes.

As one of the extensively used coating techniques, spray coating gains increasing attentions in fabricating thin films on various substrates in the fields of polymer solar cells [25,26] and super-hydrophobic coating [27–29]. Because of the facile and scalable features of spray coating to form thin coatings or multilayer films via the simple aerosolizing and depositing process, a few studies have utilized spray coating to prepare or functionalize membranes. Feng et al. modified the surface hydrophobicity of membranes by spray-coating polyaniline-silica nanoparticles for oil-water separation [30]. Hu et al. spray-coated a middle ultrathin carbon nanotube layer to promote the permeance of forward osmosis membranes [31]. Recently, our group has employed spray coating to fabricate BCP membranes by coupling it with the selective swelling process [32]. This strategy includes two steps. First, the BCP solutions are spray-coated on the macroporous nylon supports to form the composites with dense BCP layers. Then the BCP-coated supports are soaked in hot ethanol to create nanoporosities in the BCP layers following the mechanism of selective swelling-induced pore generation [11,17]. In the present study, we develop a facile approach to prepare composite BCP UF membranes, aiming to simplify the manufacturing process further. Inspired by the works devoted to preparing films in micropatterned structures [33–35], a small amount of nonsolvent is added into the BCP solutions acting as the pore-forming agent. After spray-coating the BCP solutions onto macroporous supports, the BCP layers with interconnected pores can be directly formed atop the supports, resulting in composite membranes without additional other treatments. The polysulfone-*block*-poly(ethylene glycol) (PSF-*b*-PEG) was chosen as the membrane material, given that PSF as the major block has the virtues of excellent mechanical and thermal stability, and PEG as the minor block is hydrophilic and biocompatible. This work not only provides a nondestructive strategy to introduce nanoscale porosity in BCP materials, but also demonstrates a facile, up-scalable process to produce BCP ultrafiltration membranes.

2. Experimental section

2.1. Materials

The PSF-*b*-PEG with the polydispersity index (PDI) of ~ 2.0 was obtained from Nanjing Bangding. The number-average molecular weight

(M_n) was 79.1 kDa and the weight ratio of PEG was 21%. PSF homopolymer (P3500 LCD, average molecular weight of 22 kDa) was supplied by Solvay. Analytical reagents, including tetrahydrofuran (THF, $\geq 99.5\%$), N-methyl-2-pyrrolidone (NMP, $\geq 99.0\%$), dichloromethane (DCM, $\geq 99.5\%$), 1,2-dichloroethane (DCE, $\geq 99.0\%$), acetone ($\geq 99.5\%$) and ethanol ($\geq 99.7\%$) were purchased from Shanghai Lingfeng Chemical Regent Co., Ltd. Bovine serum albumin (BSA, 98%) with a molecular weight of 66 kDa and phosphate buffer saline (PBS) tablets were purchased from MP Biomedicals, LLC. The PBS solution with pH 7.4 was obtained by dissolving one phosphate tablet in 100 mL deionized water. The nylon microfiltration membranes with a nominal pore size of ~ 0.22 μm were purchased from Haining Shenghua Filtration Equipment Co., Ltd. and used as supports to prepare composite UF membranes. Deionized water (conductivity: < 5 $\mu\text{s}\cdot\text{cm}^{-1}$) was used in all experiments. All reagents were of analytical grade and used as purchased without further purification.

2.2. Membrane preparation

The spray setup (SEV-300EDN, Suzhou Second Automatic Equipment Co., Ltd) was placed in a fume hood, and the relative humidity was varied in the range of 30–50%. The spray distance between the nozzle and the heating plate was maintained at 62 mm and the temperature of the heating plate was 25 °C. Firstly, 3 wt% PSF-*b*-PEG was ultrasonically dissolved in a solvent mixture containing small amount of water and solvent. Nylon microfiltration membranes with the size of 15 \times 15 cm^2 were fixed with two rectangular iron bars onto the horizontal heating plate of the spray setup. Afterwards, the PSF-*b*-PEG solution was poured into the reservoir of spray machine and then atomized and uniformly deposited onto nylon microfiltration membranes. The nozzle was moved forwards and backwards repeatedly, and the distance of movement was set according to the width of substrates. This spraying process was repeated until the substrate was completely covered by PSF-*b*-PEG layer (Fig. 1). The spraying time was about 2 min.

2.3. Characterizations

A field-emission scanning electron microscope (FE-SEM, Hitachi S4800) was used to detect both the surface and cross-sectional morphologies of the PSF-*b*-PEG composite membranes at an accelerating voltage of 3 kV. The membranes were quick-frozen by soaking in liquid nitrogen and ruptured to obtain the samples for cross-sectional observation. All samples were sputter-coated with gold for 20 s to avoid charging effects prior to SEM characterizations. The thicknesses of PSF-*b*-PEG layers were determined according to the cross-sectional SEM images. At least 100 pores on the surface SEM images of each samples were measured to estimate the average pore sizes by using the software Nanomeasurer. Dynamic water contact angle tests were performed to analyze the hydrophilicity of membranes by a contact angle goniometer (DropMeter A-100, Maist). The turbidity of PSF-*b*-PEG solutions were measured by Portable Turbidimeter (HACH, 2100Q).

2.4. Filtration tests and antifouling performances

Separation performances of the membranes were evaluated using a cross-flow apparatus (SF-SA, Hangzhou Saifei Membrane Separation Technique Co., Ltd.). Circular membrane coupons with a diameter of 47 mm was cut from the flat-sheet membranes to perform filtration tests. Prior to the measurements of water flux, pre-compaction of the composite membranes at 1.5 bar was carried out to ensure a stable flux. Water flux test was performed at the pressure of 1 bar. BSA solutions with the concentration of 0.5 g L^{-1} was used to evaluate the rejection ability of membranes. The BSA concentrations in feed, permeation and retentate were detected by the UV-vis feature absorption spectrometer (Nanodrop 2000C). The rejection rate of BSA was calculated according to Eq. (1):

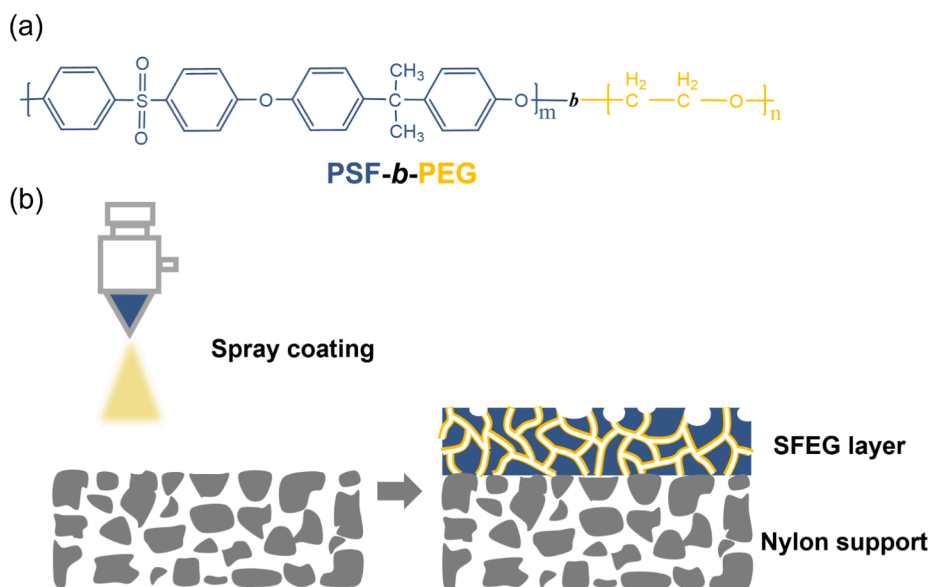


Fig. 1. (a) Molecular structure of the PSF-*b*-PEG block copolymer. (b) Preparation of PSF-*b*-PEG composite membranes by spray coating.

$$R = 100\% \times (1 - C_p/C_f) \quad (1)$$

where C_p and C_f (g L^{-1}) are BSA concentrations in the permeation and the feed solutions, respectively.

The antifouling performances of PSF-*b*-PEG membranes were investigated using BSA as a model foulant. Three alternate cycles of the deionized water and BSA solutions were performed to simulate practical membrane filtration process. The PSF-*b*-PEG membranes were thoroughly cleaned by deionized water for several times after BSA filtration. The initial water permeances of PSF-*b*-PEG membranes were marked as J_0 , the recovery water permeances of PSF-*b*-PEG membranes after BSA filtration were recorded as J_R . The water flux recovery ratio (FRR) is calculated by Eq. (2):

$$FRR = 100\% \times (J_R/J_0) \quad (2)$$

3. Results and discussion

We first investigated the mechanism of pore formation during the spray coating of water-containing PSF-*b*-PEG solutions by checking the effects of water contents and the types of used solvents.

3.1. The effect of water contents on pore formation

The nonsolvent contents in the solvent mixture have a great influence on the solubility of polymers, stability and viscosity of the solutions, which further influence the pore formation in the PSF-*b*-PEG layer. Firstly, 3 wt% PSF-*b*-PEG was dissolved in the solvent mixtures of THF with various contents of water. As shown in Fig. 2a, with the increase of water contents from 0 to 9 wt%, the PSF-*b*-PEG solutions transformed from clear and transparent (0, 3, 6 wt%) to cloudy (9 wt%) due to the decreasing solubility of PSF-*b*-PEG. The turbidity of PSF-*b*-PEG solutions with different addition of water slowly increased from 6.69 to 8.82 NTU and dramatically increased to 537.67 NTU at the end (as shown in table 2). As shown in Fig. 2b, after preserved at room temperature for one week, the PSF-*b*-PEG solutions remained homogeneous and transparent when the water contents were 0 wt%, 3 wt% and 6 wt%. In contrast, PSF-*b*-PEG was precipitated (marked by yellow box in Panel b) when the water content was 9 wt%.

The PSF-*b*-PEG solutions with different water contents were directly spray-coated on silicon substrates under identical conditions. As shown in Fig. 3a and e, nanopores can be only observed on the surface of PSF-*b*-

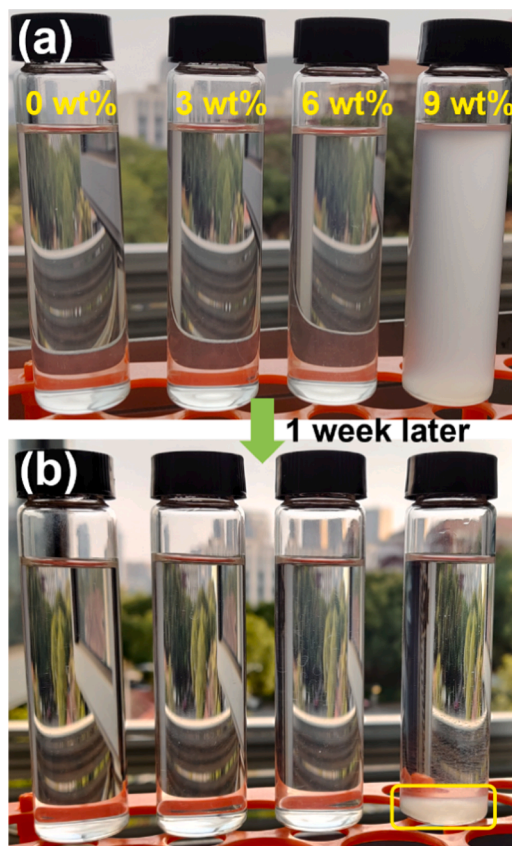


Fig. 2. (a) The images of PSF-*b*-PEG dissolved in solvent mixture containing different percentages of water and (b) the solutions preserved at room temperature for one week.

PEG layer and hardly distributed throughout the whole PSF-*b*-PEG layer when no water in SEFG solutions. With the water content increased to 3 wt%, abundant of macropores and mesopores appeared on the surface of PSF-*b*-PEG layer and these interconnected pores spanned the whole PSF-*b*-PEG layer as shown in Fig. 3b and f. While the PSF-*b*-PEG tended to aggregate as micelles and stacked on the silicon substrates after water

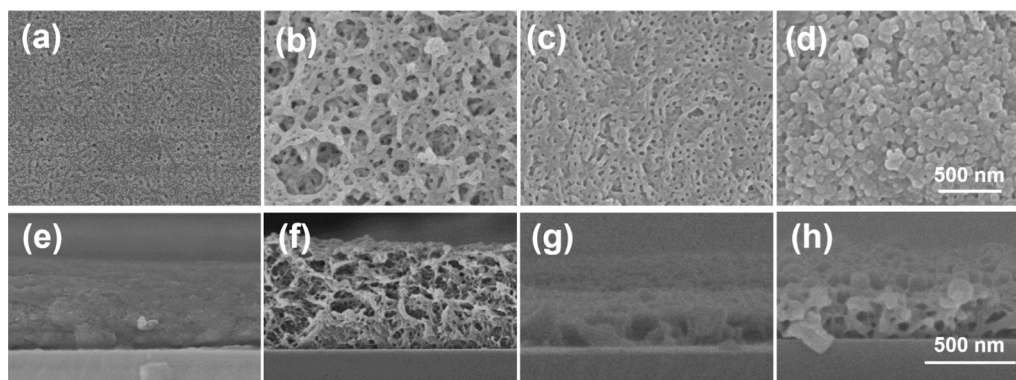


Fig. 3. The SEM images of PSF-*b*-PEG layers directly spray-coated on silicon substrates: (a–d) surface and (e–h) cross-sectional morphologies with water contents varying from 0, 3, 6 to 9 wt%, respectively. Images of (a–d) have the same magnification and the scale bar corresponding to 500 nm is given in (d). Images of (e–h) have the same magnification and the scale bar corresponding to 500 nm is given in (h).

contents were increased to 6 and 9 wt% (Fig. 3c, d, g and h). It seems like that nonsolvent of water acted as porogen to form pores after completely evaporation. However, the increasing of water content (9 wt%) will destroy the homogeneity of (PSF-*b*-PEG)-THF system and cause micellization. It should be noted that the PSF-*b*-PEG layer was still formed from micelles while extracting the supernatant of PSF-*b*-PEG solution (9 wt% water content and preserved for one week) to spray, indicating that the preservation would not change the morphology of produced films.

3.2. The effect of solvent types on pore formation

The solvent used to dissolve PSF-*b*-PEG is one of the primary parameters influencing the nanostructures of the eventually obtained PSF-*b*-PEG membranes. Here, in order to figure out the role of solvent in the pore formation process, other four types of solvent with changing boiling point and water miscibility (Table 1) were chosen to mix with water.

3 wt% water was added into different solvents (DCE, NMP, DCM and acetone) to prepare the binary solvent mixtures. Subsequently, PSF-*b*-PEG (3 wt%) was dissolved in the solvent mixtures. As shown in Fig. S1a, c and d, it was hard to obtain a transparent PSF-*b*-PEG solution though only small amounts of nonsolvent (water) was mixed with solvents except for the water-miscible NMP (Fig. S1b). Besides, PSF-*b*-PEG dissolved in the mixture of water and acetone formed micelles as shown in Fig. S1d. After preserved at room temperature for one week, precipitates appeared in all SEFG solutions as shown in Fig. S1e, g and h. The precipitate was in the bottom when the density of the solvent was lower than the density of water, otherwise the precipitate was floating on the solvents surface. Consequently, it can be inferred that PSF-*b*-PEG matrix was enveloped by water and separated with solvents because of strong affinity between water and PEG chains. Besides, as shown in Fig. S1f, the PSF-*b*-PEG solution using a solvent mixture of NMP and H₂O kept transparent and clear. That owes to the excellent solubility to PSF-*b*-PEG and good miscibility of water and NMP.

The PSF-*b*-PEG solutions with different kinds of solvent mixtures were directly spray-coated on the silicon substrates under the identical conditions. As shown in Fig. 4a and e, there was no porous structure generated in the whole PSF-*b*-PEG layer due to the poor miscibility of DCE with H₂O. It gives a clue that water is hard to homogeneously mix with (PSF-*b*-PEG)-DCE system and act as pore-forming agent for

Table 1
Physical parameters of different solvents.

Solvent	H ₂ O	THF	DCE	NMP	DCM	Acetone
Boiling point (°C)	100	66	83.5	202	39.8	56.5
Water miscibility	/	YES	NO	YES	NO	YES
Density (g mL ⁻¹)	1.000	0.890	1.235	1.026	1.325	0.738

Table 2
Turbidity of PSF-*b*-PEG solutions containing different water contents.

Water contents (wt %)	0	3	6	9
Turbidity (NTU)	6.69 ± 0.05	7.04 ± 0.13	8.82 ± 0.12	537.67 ± 0.58

nanoporous structure. As shown in Fig. 4b and f, even though NMP is a good solvent for PSF-*b*-PEG and can be miscible with H₂O, porous structure was hardly created in the PSF-*b*-PEG layer owing to the poor volatility of NMP. The evaporation rate of water was faster than NMP in the process of PSF-*b*-PEG solidification. It was hard to preserve the pore volume before PSF-*b*-PEG was completely solidified. For the mixed solvent of DCM and H₂O, nanopores was observed on the surface of PSF-*b*-PEG layer as shown in Fig. 4c, but they were hardly distributed in the interior of the PSF-*b*-PEG layer (Fig. 4g). This may be attributed to the high volatility of DCM at room temperature and its immiscibility with H₂O. The high evaporation rate of DCM is helpful to condense moisture in the air and form pores on the surface of PSF-*b*-PEG layer. However, water is hard to homogeneously mix with (PSF-*b*-PEG)-DCM system and act as the porogen to obtain a continuous porous structure. PSF-*b*-PEG with a concentration of 3 wt% is hard to be completely dissolved in the mixed solvent of acetone and H₂O. They formed spherical micelles with the hydrophilic PEG coronas and hydrophobic PSF cores in the mixed solvent of acetone and H₂O [36]. After spray coating, PSF-*b*-PEG spherical micelles were tightly stacked on the silicon substrates as shown in Fig. 4d and h.

Considering that PSF-*b*-PEG dissolved in the solvent mixture of THF and H₂O was the only successful case to form interconnected porous structure, it can be known that water is able to homogeneously disperse with (PSF-*b*-PEG)-solvent system and act as porogen for the formation of interconnected porous structure. Besides, water should be preserved in the PSF-*b*-PEG layers before solvent evaporation, i.e., the evaporation rates of solvents should be faster than water. Herein, prerequisites of the solvents to generate interconnected pores throughout the whole PSF-*b*-PEG layer should be: (I) Rapid evaporation rate; (II) Good miscibility with water.

3.3. The effect of PEG chains on pore formation

PSF homopolymer was employed as a comparison to illuminate the effect of hydrophilic PEG chains on pore formation. 3 wt% PSF was dissolved in the mixed solvent containing 3 wt% water and 94 wt% THF. Under the same spray-coating conditions, no pores were observed on the surface or in the interior of the produced PSF-*b*-PEG coated film (Fig. S2). Therefore, we conclude that PEG chains in PSF-*b*-PEG adsorb

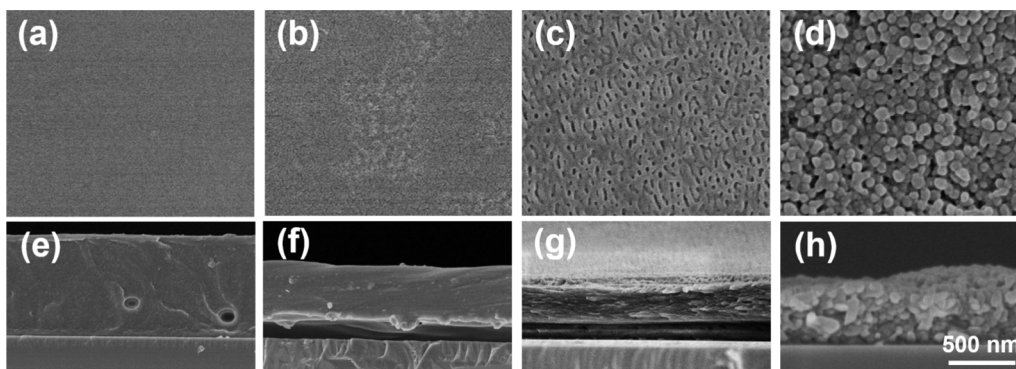


Fig. 4. The surface (a–d) and cross-sectional (e–h) SEM images of PSF-*b*-PEG layers spray-coated on the silicon substrates prepared with different mixed solvents: H₂O + DCE, H₂O + NMP, H₂O + DCM, H₂O + acetone, respectively. All images have the same magnification and the scale bar corresponding to 500 nm is given in (h).

and stabilize water droplets and moisture because of their strong affinity to water. That is, water droplets can be held by PEG chains before transforming into porous structure by evaporation. Consequently, PSF solutions cannot produce porous structure by spray coating because of the lack of PEG chains.

3.4. Mechanism of pore formation

We proposed that the PSF-*b*-PEG pore-generation mechanism during spray coating might be: (I) When the PSF-*b*-PEG solutions were atomized into numerous microdroplets and sprayed from the nozzle tip to the substrate plate, highly volatile THF was mostly evaporated while water largely remained. (II) Tiny water droplets began to separate out from the PSF-*b*-PEG matrix. Meanwhile, the growth and coalescence of water droplets will accelerate the size of phase separation. Subsequently, solutions droplets containing water droplets were collided and merged with each other to form a thin and continuous PSF-*b*-PEG layer when deposited on substrate. (III) Finally, the water was evaporated and the PSF-*b*-PEG matrix was solidified. The space occupied by water droplets was transformed into mesopores, which fully span the whole thickness of the PSF-*b*-PEG layer. As shown in Fig. 1 and 5, water droplets begin to nucleate at the initial stage and grow during spraying from the nozzle tip to the substrate plate. Consequently, different sizes of mesopores were generated in the process of nucleation and growth of water droplets. Besides, the macropores might be a result of air vortex during solution

droplets sprayed onto the substrates.

3.5. Preparation of PSF-*b*-PEG composite membranes

As we demonstrate above, interconnected porosities can be efficiently produced in PSF-*b*-PEG layers simply by spray-coating PSF-*b*-PEG solutions containing small amount of nonsolvent (H₂O, 3 wt%). This allows us to prepare composite membranes with the porous PSF-*b*-PEG coating as the separation layer by spray-coating the solution on macroporous substrates. The macroporous nylon support (Fig. 6a) can be completely covered by the nanoporous PSF-*b*-PEG layer to form a composite membrane (Fig. 6c and d). There were two types of pores with different sizes in the PSF-*b*-PEG layer: macropores and mesopores. It is worth noting that mesopores (average size of 22 nm) span the whole PSF-*b*-PEG layers, while macropores only scatter on the surface of PSF-*b*-PEG layers. Clearly, the PSF-*b*-PEG composite membranes have a bilayered structure composed by the nylon support and the PSF-*b*-PEG top layer (Fig. 6b). The interconnected PSF-*b*-PEG network was firmly attached with the frameworks of the nylon support (Fig. 6e), ensuring a strong mechanical strength of the composite structure. Besides, a free-standing porous PSF-*b*-PEG layer can be detached from the silicon or glass substrate, and also showed good mechanical strength even through the thickness of the PSF-*b*-PEG layer was as thin as ~500 nm (Fig. 6h), primarily owing to the robust PSF matrix.

It should be noted that porous structure would collapse when the

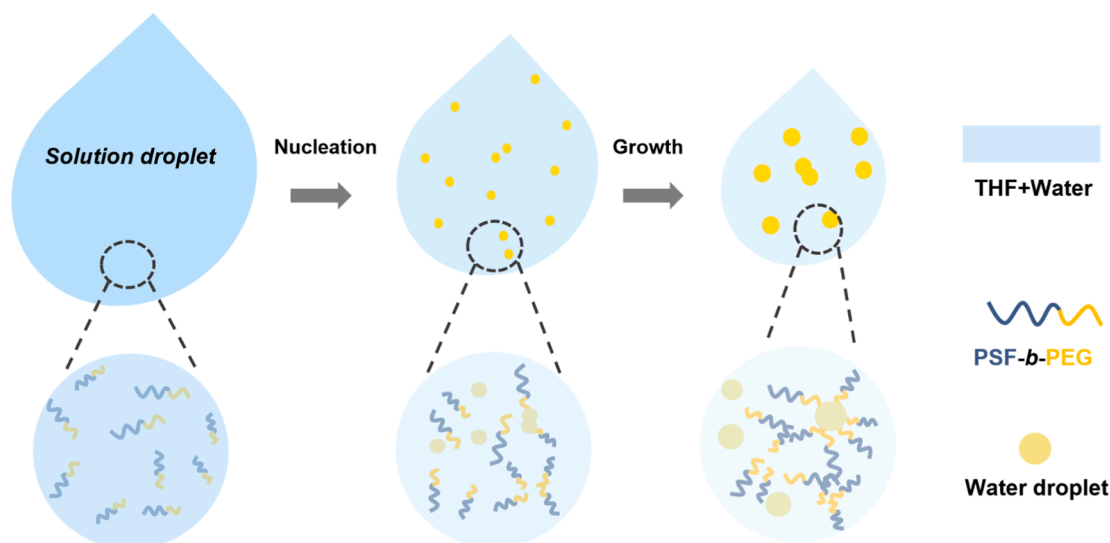


Fig. 5. Schematic diagram of the evolution process of water droplet during spray coating.

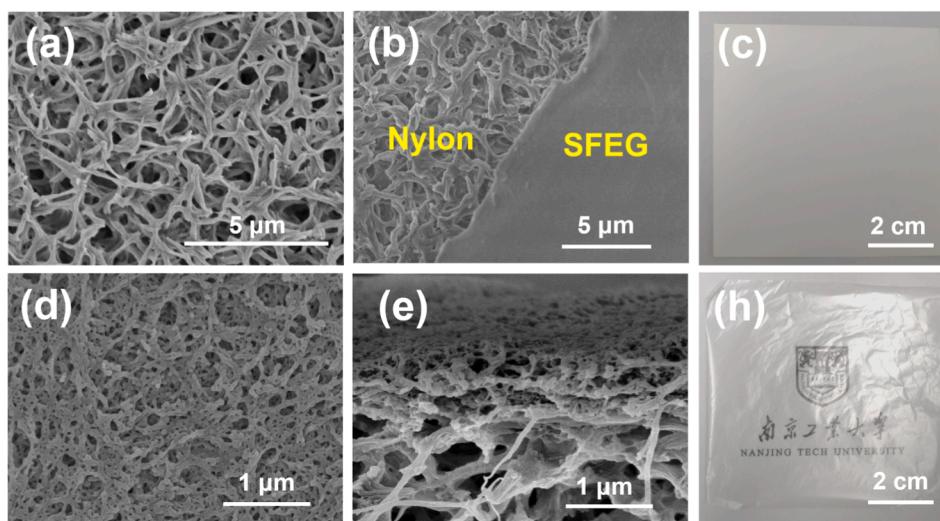


Fig. 6. The SEM images of (a) nylon substrate, (b) the composite structure of PSF-*b*-PEG membrane, (d) top-view and (e) cross-sectional view of the SEFG composite membrane; The digital images of (c) PSF-*b*-PEG composite membrane and (h) the free-standing PSF-*b*-PEG membrane.

PSF-*b*-PEG composite membranes were immediately dried in the oven at 100 °C for 30 min after spray coating. However, when the spray-coated membranes were dried at room temperature for 24 h first, the porous structure could be retained even though heating treatment to the membranes at 100 °C for 30 min was performed, as shown in Fig. S3. Therefore, it is reasonable to deduce that porous structure is resulted from the volumes occupied by water. An immediate heating treatment after spray-coating will evaporate the water before the PSF-*b*-PEG phases are completely solidified, which destroys the porous structure.

3.6. UF performances of PSF-*b*-PEG composite membranes

By controlling the deposition volumes of SEFG solutions, the thickness of PSF-*b*-PEG layer can be facilely controlled to tune the separation performances. The surface of PSF-*b*-PEG composite membranes prepared with different deposition volumes almost have same morphologies. With the deposition volumes of PSF-*b*-PEG solutions increased from 2 to 9, 13.5 and 18 $\mu\text{L cm}^{-2}$, the thicknesses of PSF-*b*-PEG layers were increased from 0.45 to 1.07, 2.06 and 3.30 μm , respectively. (Fig. 7 and Fig. S4).

The surface hydrophilicity of PSF-*b*-PEG membranes was evaluated by water contact angle tests. As shown in Fig. 8, the water contact angles of PSF-*b*-PEG membranes were 74, 71.8, 78.4 and 74.5° with the PSF-*b*-PEG deposition volumes varied from 2 to 9, 13.5 and 18 $\mu\text{L cm}^{-2}$ respectively. The values of contact angles of PSF-*b*-PEG membranes were

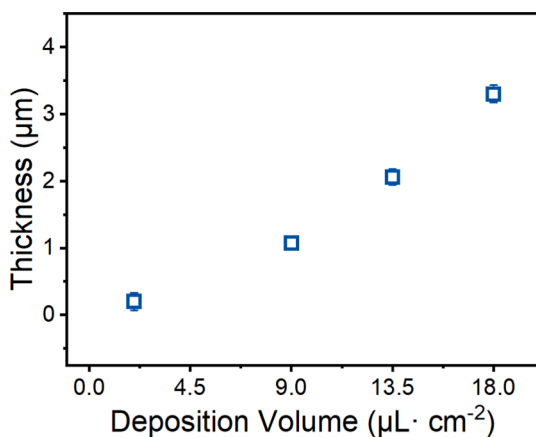


Fig. 7. The thicknesses of PSF-*b*-PEG layers varied with deposition volumes.

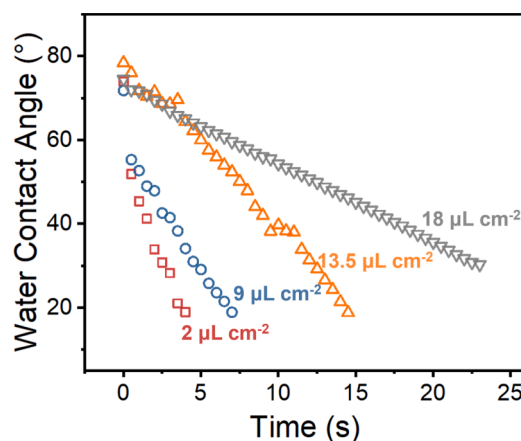


Fig. 8. Dynamic water contact angles of the PSF-*b*-PEG composite membranes with various solutions deposition volumes.

lower than PSF homopolymer (92.9°). As discussed above, the PEG chains in PSF-*b*-PEG were spontaneously enriched on the pore surface during absorbing and stabilizing water droplets, which is good for high water permeance. Besides, the durations for water droplets to penetrate the membranes were increased from 5 to 30 s in the testing of dynamic contact angles. These results demonstrate that the surface hydrophilicity of PSF-*b*-PEG membranes fabricated with various PSF-*b*-PEG deposition volumes were similar. However, the water transport ability was inverse to the thickness of PSF-*b*-PEG layer.

The performances of PSF-*b*-PEG composite membranes were assessed by pure water flux and BSA solutions. As shown in Fig. 9a, the nylon support had a water permeance of about 2267 $\text{L}\cdot\text{m}^{-2}\cdot\text{h}^{-1}\cdot\text{bar}^{-1}$ and a negligible BSA rejection rate of 5.4%. With the spraying doses of PSF-*b*-PEG solutions increased from 2 to 18 $\mu\text{L}\cdot\text{cm}^{-2}$, the water permeances of the PSF-*b*-PEG composite membranes were lowered from 592 to 59 $\text{L}\cdot\text{m}^{-2}\cdot\text{h}^{-1}\cdot\text{bar}^{-1}$ and the BSA rejection rates were raised from 45 to 71%, owing to the increased thicknesses of PSF-*b*-PEG separation layers. *FRR* tests were carried out to show the anti-fouling ability of PSF-*b*-PEG composite membranes. As shown in Fig. 9b, the *FRR* of membrane was about 89.6% after BSA fouling in the first test circle and then exhibited little changes with a *FRR* value of 86.9% in the third test cycle. This flux recovery ratio is higher than PSF membranes [37] owing to the hydrophilic PEG chains of PSF-*b*-PEG. Water permeance variation tests were

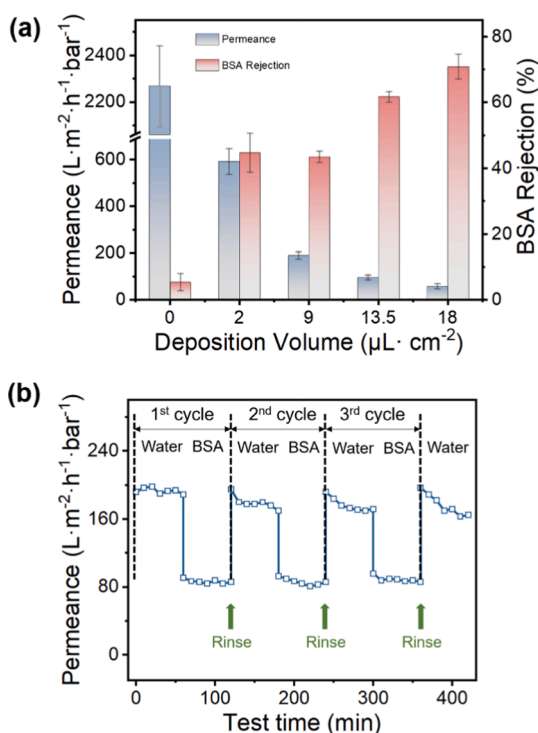


Fig. 9. (a) The permeances and BSA rejections of the PSF-*b*-PEG composite membranes with various solutions deposition volumes. (b) The anti-fouling ability test of the PSF-*b*-PEG composite membrane with a deposition volume of 9 $\mu\text{L} \cdot \text{cm}^{-2}$.

performed to show the stability of membranes. As shown in Fig. S6, water flux decreased by 25.8% in the first 1 h test and finally got stable around 371 $\text{L} \cdot \text{m}^{-2} \cdot \text{h}^{-1} \cdot \text{bar}^{-1}$. Considering the highly porous structure of the PSF-*b*-PEG layer, such a moderate decrease in permeance is reasonable and acceptable.

The adhesion between the PSF-*b*-PEG layer and nylon support was evaluated by immersing the PSF-*b*-PEG composite membranes into a shaking water at the ultrasonic power of 100 W for 30 min. As shown in Fig. S5, there was no exfoliation of PSF-*b*-PEG layer from the support. Meanwhile, the composite membranes after ultrasonic processing possessed almost identical water permeance and BSA rejection compared with the pristine membranes, indicating that the PSF-*b*-PEG layers were firmly attached to the nylon supports after spray coating.

4. Conclusions

In summary, we have demonstrated a facile process for the fabrication of block copolymer UF membranes with good ultrafiltration performances and fouling resistance. The pore formation of PSF-*b*-PEG layer is strongly influenced by the water content and the type of solvents. The presence of hydrophilic PEG chains in PSF-*b*-PEG copolymer is essential for the formation of pores as PEG chains stabilize water droplets. To generate interconnected pores throughout the whole PSF-*b*-PEG layers for ultrafiltration, the solvents should have rapid evaporation rate than water and good miscibility with water. Water is nonsolvent and can be homogeneously mixed in the PSF-*b*-PEG-solvent system and act as pore-forming agent during PSF-*b*-PEG solidification. Water content should be controlled in an appropriate level, too more and too less are both adverse for generating pores in the PSF-*b*-PEG layer. The thicknesses of PSF-*b*-PEG layers can be readily tuned by controlling the deposition volumes of PSF-*b*-PEG solutions, resulting in adjustable performances of PSF-*b*-PEG composite membranes. With the deposition volumes of PSF-*b*-PEG solutions varied from 2 to 13.5 $\mu\text{L} \cdot \text{cm}^{-2}$, the water permeances change from 592 to 59 $\text{L} \cdot \text{m}^{-2} \cdot \text{h}^{-1} \cdot \text{bar}^{-1}$ and the BSA rejections are

increased from 45 to 71%. As PEG chains are enriched on the pore walls, the membrane surface is hydrophilic and exhibits excellent fouling resistance to proteins. As the pore-making process by doping water in amphiphilic copolymers and spray coating can be easily realized and flexibly controlled, this work provides a simple and potentially upscalable strategy to produce BCP ultrafiltration membranes. Also, it should be aware of that dilute BCP solutions are required in the spray coating process to ensure low viscosity for smooth coating and also thin selective layers of the produced composite membranes. Therefore, future work should be focused to develop solutions using water as the solvent to reduce the use of organic solvents.

CRediT authorship contribution statement

Dongwei Ma: Methodology, Investigation, Data curation, Writing - original draft. **Xiangyue Ye:** Investigation, Methodology. **Zhuo Li:** Investigation, Methodology. **Jiemei Zhou:** Writing - review & editing, Validation, Supervision. **Dinglei Zhong:** Investigation, Methodology. **Chenxu Zhang:** Investigation, Methodology, Validation. **Sen Xiong:** Investigation, Methodology, Validation. **Jianzhong Xia:** Investigation, Methodology, Supervision. **Yong Wang:** Conceptualization, Supervision.

Declaration of Competing Interest

The authors declare that they have no known competing financial interests or personal relationships that could have appeared to influence the work reported in this paper.

Acknowledgments

Financial support from the National Natural Science Foundation of China (21706119) and the Program of Excellent Innovation Teams of Jiangsu Higher Education Institutions and the Project of Priority Academic Program Development of Jiangsu Higher Education Institutions (PAPD) is gratefully acknowledged.

Appendix A. Supplementary material

Supplementary data to this article can be found online at <https://doi.org/10.1016/j.seppur.2020.118100>.

References

- [1] D. Wu, F. Xu, B. Sun, R. Fu, H. He, K. Matyjaszewski, Design and preparation of porous polymers, *Chem. Rev.* 112 (2012) 3959–4015.
- [2] J.R. Werber, C.O. Osuji, M. Elimelech, Materials for next-generation desalination and water purification membranes, *Nat. Rev. Mater.* 1 (2016) 16037.
- [3] A. Lee, J.W. Elam, S.B. Darling, Membrane materials for water purification: design, development, and application, *Environ. Sci. Water Res. Technol.* 2 (2016) 17–42.
- [4] J.K. Kim, S.Y. Yang, Y. Lee, Y. Kim, Functional nanomaterials based on block copolymer self-assembly, *Prog. Polym. Sci.* 35 (2010) 1325–1349.
- [5] S.B. Darling, Directing the self-assembly of block copolymers, *Prog. Polym. Sci.* 32 (2007) 1152–1204.
- [6] K.V. Peinemann, V. Abetz, P.F. Simon, Asymmetric superstructure formed in a block copolymer via phase separation, *Nat. Mater.* 6 (2007) 992–996.
- [7] M. Radjabian, V. Abetz, Advanced porous polymer membranes from self-assembling block copolymers, *Prog. Polym. Sci.* 102 (2020) 101219.
- [8] Y. Zhang, J.L. Sargent, B.W. Boudouris, W.A. Phillip, Nanoporous membranes generated from self-assembled block polymer precursors: Quo Vadis? *J. Appl. Polym. Sci.* 132 (2015) 41683–41700.
- [9] L. Upadhyaya, M. Semsarilar, S. Nehache, A. Deratani, D. Quemener, Filtration membranes from self-assembled block copolymers – a review on recent progress, *Eur. Phys. J. Spec. Top.* 224 (2015) 1883–1897.
- [10] S.P. Nunes, P.Z. Culfaz-Emecen, G.Z. Ramon, T. Visser, G.H. Koops, W. Jin, M. Ulbricht, Thinking the future of membranes: perspectives for advanced and new membrane materials and manufacturing processes, *J. Membr. Sci.* 598 (2020) 117761.
- [11] Y. Wang, C. He, W. Xing, F. Li, L. Tong, Z. Chen, X. Liao, M. Steinhart, Nanoporous metal membranes with bicontinuous morphology from recyclable block-copolymer templates, *Adv. Mater.* 22 (2010) 2068–2072.

- [12] S.Y. Yang, I. Ryu, H.Y. Kim, J.K. Kim, S.K. Jang, T.P. Russell, Nanoporous membranes with ultrahigh selectivity and flux for the filtration of viruses, *Adv. Mater.* 18 (2006) 709–712.
- [13] D.A. Olson, L. Chen, M.A. Hillmyer, Templating nanoporous polymers with ordered block copolymers, *Chem. Mater.* 20 (2008) 869–890.
- [14] U. Jeong, D.Y. Ryu, D.H. Kho, J.K. Kim, J.T. Goldbach, D.H. Kim, T.P. Russell, Enhancement in the orientation of the microdomain in block copolymer thin films upon the addition of homopolymer, *Adv. Mater.* 16 (2004) 533–536.
- [15] W.A. Phillip, B. O'Neill, M. Rodwogin, M.A. Hillmyer, E.L. Cussler, Self-assembled block copolymer thin films as water filtration membranes, *ACS Appl. Mater. Interfaces* 2 (2010) 847–853.
- [16] F. Guo, J.W. Andreasen, M.E. Vigild, S. Ndoni, Influence of 1,2-PB matrix cross-linking on structure and properties of selectivity etched 1,2-PB-b-PDMS block copolymer, *Macromolecules* 40 (2007) 3669–3675.
- [17] Y. Wang, Nondestructive creation of ordered nanopores by selective swelling of block copolymers: toward homoporous membranes, *Acc. Chem. Res.* 49 (2016) 1401–1408.
- [18] Z. Wang, L. Guo, Y. Wang, Isoporous membranes with gradient porosity by selective swelling of UV-crosslinked block copolymers, *J. Membr. Sci.* 476 (2015) 449–456.
- [19] M. Wei, W. Sun, X. Shi, Z. Wang, Y. Wang, Homoporous membranes with tailored pores by soaking block copolymer/homopolymer blends in selective solvents: dissolution versus swelling, *Macromolecules* 49 (2015) 215–223.
- [20] N. Yan, Z. Wang, Y. Wang, Highly permeable membranes enabled by film formation of block copolymers on water surface, *J. Membr. Sci.* 568 (2018) 40–46.
- [21] L. Guio, C. Liu, D. Boures, P.T. Getty, R. Waldman, X. Liu, S.B. Darling, Procedure for the transfer of polymer films onto porous substrates with minimized defects, *J. Visual. Exp.* 148 (2019) 2–9.
- [22] X. Shi, Z. Wang, Y. Wang, Highly permeable nanoporous block copolymer membranes by machine-casting on nonwoven supports: an upscalable route, *J. Membr. Sci.* 533 (2017) 201–209.
- [23] Z. Wang, X. Yao, Y. Wang, Swelling-induced mesoporous block copolymer membranes with intrinsically active surfaces for size-selective separation, *J. Mater. Chem.* 22 (2012) 20542–20548.
- [24] X. Yao, L. Guo, X. Chen, J. Huang, M. Steinhart, Y. Wang, Filtration-based synthesis of micelle-derived composite membranes for high-flux ultrafiltration, *ACS Appl. Mater. Interfaces* 7 (2015) 6974–6981.
- [25] L.L.N. Andrea Reale, Luigi Salamandra, Giuseppina Polino, Gianpaolo Susanna, Thomas M. Brown, Francesca Brunetti, Aldo Di Carlo, Spray coating for polymer solar cells: an up-to-date overview, *Energy Technol.* 3 (2015) 385–406.
- [26] C. Grotto, B.P. Rand, J. Genoe, P. Heremans, Exploring spray coating as a deposition technique for the fabrication of solution-processed solar cells, *Sol. Energy Mater. Sol. Cells* 93 (2009) 454–458.
- [27] H. Ye, L. Zhu, W. Li, H. Liu, H. Chen, Simple spray deposition of a water-based superhydrophobic coating with high stability for flexible applications, *J. Mater. Chem. A* 5 (2017) 9882–9890.
- [28] K. Sasaki, M. Tenjimbayashi, K. Manabe, S. Shiratori, Asymmetric superhydrophobic/superhydrophilic cotton fabrics designed by spraying polymer and nanoparticles, *ACS Appl. Mater. Interfaces* 8 (2016) 651–659.
- [29] D.Y. Guo, J.H. Chen, L.F. Wen, P. Wang, S.P. Xu, J. Cheng, X.F. Wen, S.F. Wang, C. Y. Huang, P.H. Pi, A superhydrophobic polyacrylate film with good durability fabricated via spray coating, *J. Mater. Sci.* 53 (2018) 15390–15400.
- [30] W. Zhang, X. Li, R. Qu, Y. Liu, Y. Wei, L. Feng, Janus membrane decorated via a versatile immersion-spray route: controllable stabilized oil/water emulsion separation satisfying industrial emission and purification criteria, *J. Mater. Chem. A* 7 (2019) 4941–4949.
- [31] Z.Y. Zhou, Y.X. Hu, C. Boo, Z.Y. Liu, J.Q. Li, L.Y. Deng, X.C. An, High-performance thin-film composite membrane with an ultrathin spray-coated carbon nanotube interlayer, *Environ. Sci. Technol. Lett.* 5 (2018) 243–248.
- [32] D. Ma, J. Zhou, Z. Wang, Y. Wang, Block copolymer ultrafiltration membranes by spray coating coupled with selective swelling, *J. Membr. Sci.* 598 (2020) 117656.
- [33] Y. Wang, Z. Liu, B. Han, H. Gao, J. Zhang, X. Kuang, A simple route to micropatterned polymer surfaces, *Chem. Commun.* 7 (2004) 800–801.
- [34] Y. Wang, Z. Liu, B. Han, Z. Sun, J. Zhang, D. Sun, Phase-separation-induced micropatterned polymer surfaces and their applications, *Adv. Funct. Mater.* 15 (2005) 655–663.
- [35] Y. Wang, Z. Liu, Y. Huang, B. Han, G. Yang, Micropatterned polymer surfaces induced by nonsolvent, *Langmuir* 22 (2006) 1928–1931.
- [36] Z. Zhang, J. Li, Z. Wang, C. He, Y. Wang, Polymeric nanospheres with tunable sizes, water dispersibility, and thermostability from heating-enabled micellization of polysulfone-block-polyethylene glycol, *J. Polym. Sci., Part B: Polym. Phys.* 56 (2018) 769–777.
- [37] N. Wang, T. Wang, Y.X. Hu, Tailoring membrane surface properties and ultrafiltration performances via the self-assembly of polyethylene glycol-block-polysulfone-block-polyethylene glycol block copolymer upon thermal and solvent annealing, *ACS Appl. Mater. Interfaces* 9 (2017) 31018–31030.